Mobius3D

THE COMPLETE PATIENT QA SYSTEM

- **3D PATIENT PLAN QA**
- **3D IMRT/VMAT PRE TREATMENT QA**
- **3D *IN VIVO* DAILY TREATMENT QA**
- **ONLINE PATIENT POSITIONING QA**

Upgrade your patient safety by bridging the gap between patient QA and machine QA:

DoseLab, the complete TG-142 solution, is now integrated into Mobius3D!

Visit mobiusmed.com/mobius3d to learn more or register for a bi-weekly webinar at mobiusmed.com/webinars

MOBIUS MEDICAL SYSTEMS
INNOVATIVE SOFTWARE FOR MODERN RADIATION ONCOLOGY

Low-frequency quantitative ultrasound imaging of cell death *in vivo*

Ali Sadeghi-Naini
Imaging Research – Physical Science, Sunnybrook Research Institute, Sunnybrook Health Sciences Centre, Toronto, Ontario M4N 3M5, Canada; Department of Radiation Oncology, Odette Cancer Centre, Sunnybrook Health Sciences Centre, Toronto, Ontario M4N 3M5, Canada; Department of Medical Biophysics, Faculty of Medicine, University of Toronto, Toronto, Ontario M4N 3M5, Canada; and Department of Radiation Oncology, Faculty of Medicine, University of Toronto, Toronto, Ontario M4N 3M5, Canada

Naum Papanicolau
Imaging Research – Physical Science, Sunnybrook Research Institute, Sunnybrook Health Sciences Centre, Toronto, Ontario M4N 3M5, Canada and Department of Medical Biophysics, Faculty of Medicine, University of Toronto, Toronto, Ontario M4N 3M5, Canada

Omar Falou
Imaging Research – Physical Science, Sunnybrook Research Institute, Sunnybrook Health Sciences Centre, Toronto, Ontario M4N 3M5, Canada; Department of Radiation Oncology, Odette Cancer Centre, Sunnybrook Health Sciences Centre, Toronto, Ontario M4N 3M5, Canada; Department of Medical Biophysics, Faculty of Medicine, University of Toronto, Toronto, Ontario M4N 3M5, Canada; and Department of Radiation Oncology, Faculty of Medicine, University of Toronto, Toronto, Ontario M4N 3M5, Canada

Hadi Tadayyon
Imaging Research – Physical Science, Sunnybrook Research Institute, Sunnybrook Health Sciences Centre, Toronto, Ontario M4N 3M5, Canada and Department of Medical Biophysics, Faculty of Medicine, University of Toronto, Toronto, Ontario M4N 3M5, Canada

Justin Lee
Department of Radiation Oncology, Odette Cancer Centre, Sunnybrook Health Sciences Centre, Toronto, Ontario M4N 3M5, Canada and Department of Radiation Oncology, Faculty of Medicine, University of Toronto, Toronto, Ontario M4N 3M5, Canada

Judit Zubovits
Department of Pathology, Sunnybrook Health Sciences Centre, Toronto, Ontario M4N 3M5, Canada

Alireza Sadeghian
Department of Computer Science, Ryerson University, Toronto, Ontario M5B 2K3, Canada

Raffi Karshafian
Department of Physics, Ryerson University, Toronto, Ontario M5B 2K3, Canada

Azza Al-Mahrouki and Anoja Giles
Imaging Research – Physical Science, Sunnybrook Research Institute, Sunnybrook Health Sciences Centre, Toronto, Ontario M4N 3M5, Canada and Department of Radiation Oncology, Odette Cancer Centre, Sunnybrook Health Sciences Centre, Toronto, Ontario M4N 3M5, Canada

Michael C. Kolios
Department of Medical Biophysics, Faculty of Medicine, University of Toronto, Toronto, Ontario M4N 3M5, Canada and Department of Physics, Ryerson University, Toronto, Ontario M5B 2K3, Canada

Gregory J. Czarnota[a)]
Imaging Research – Physical Science, Sunnybrook Research Institute, Sunnybrook Health Sciences Centre, Toronto, Ontario M4N 3M5, Canada; Department of Radiation Oncology, Odette Cancer Centre, Sunnybrook Health Sciences Centre, Toronto, Ontario M4N 3M5, Canada; Department of Medical Biophysics, Faculty of Medicine, University of Toronto, Toronto, Ontario M4N 3M5, Canada; and Department of Radiation Oncology, Faculty of Medicine, University of Toronto, Toronto, Ontario M4N 3M5, Canada

(Received 10 December 2012; revised 12 June 2013; accepted for publication 14 June 2013; published 11 July 2013)

Purpose: Currently, no clinical imaging modality is used routinely to assess tumor response to cancer therapies within hours to days of the delivery of treatment. Here, the authors demonstrate the efficacy of ultrasound at a clinically relevant frequency to quantitatively detect changes in tumors in response to cancer therapies using preclinical mouse models.

Methods: Conventional low-frequency and corresponding high-frequency ultrasound (ranging from 4 to 28 MHz) were used along with quantitative spectroscopic and signal envelope statistical analyses on data obtained from xenograft tumors treated with chemotherapy, x-ray radiation, as well as a novel vascular targeting microbubble therapy.

Results: Ultrasound-based spectroscopic biomarkers indicated significant changes in cell-death associated parameters in responsive tumors. Specifically changes in the midband fit, spectral slope,

and 0-MHz intercept biomarkers were investigated for different types of treatment and demonstrated cell-death related changes. The midband fit and 0-MHz intercept biomarker derived from low-frequency data demonstrated increases ranging approximately from 0 to 6 dBr and 0 to 8 dBr, respectively, depending on treatments administrated. These data paralleled results observed for high-frequency ultrasound data. Statistical analysis of ultrasound signal envelope was performed as an alternative method to obtain histogram-based biomarkers and provided confirmatory results. Histological analysis of tumor specimens indicated up to 61% cell death present in the tumors depending on treatments administered, consistent with quantitative ultrasound findings indicating cell death. Ultrasound-based spectroscopic biomarkers demonstrated a good correlation with histological morphological findings indicative of cell death ($r^2 = 0.71, 0.82$; $p < 0.001$).

Conclusions: In summary, the results provide preclinical evidence, for the first time, that quantitative ultrasound used at a clinically relevant frequency, in addition to high-frequency ultrasound, can detect tissue changes associated with cell death *in vivo* in response to cancer treatments. © *2013 American Association of Physicists in Medicine*. [http://dx.doi.org/10.1118/1.4812683]

Key words: cell death, apoptosis, mitotic arrest, ultrasound, spectroscopy, antivascular therapy, radiation therapy, chemotherapy

1. INTRODUCTION

The principle aim of cancer therapy is to induce cell death within a target tumor in order to destroy it. Current methods of assessing therapy effects during patient treatment are often invasive, requiring cytometric analysis of biopsied tissue. Commonly used clinical assessments, including imaging, are primarily based upon tumor size measurements. Nevertheless, tumor-size reduction can often require several weeks to months of treatment and in some cases tissue diminishment is not present despite a positive treatment response.[1] The development of a noninvasive manner to monitor patient responses to therapy would be advantageous in order to guide the customization of chemotherapy or other cancer therapies. If limited or no cell death is detected in response to therapy, clinicians would be able to potentially alter an ineffective treatment, changing it to a more efficacious one. This could take place early following the start of a treatment (days to weeks) as opposed to continuing ineffective treatments for months. A number of imaging modalities have been investigated to permit such evaluations including magnetic resonance imaging, positron emission tomography, and other methods.[1–5] In this study, we investigate for the first time the potential of conventional-frequency quantitative ultrasound-based biomarkers to noninvasively monitor the effects of cancer therapies in mouse tumor models *in vivo*.

Quantitative ultrasound techniques are predicated, in part, on those methods which analyze ultrasound radiofrequency (RF) raw data, before it is envelope detected, log amplified, and processed to form a B-mode US image, in order to extract quantitative measures describing acoustic characteristics of the scanned tissue. Such techniques frequently apply calibration and/or normalization techniques in order to derive parameter estimates from ultrasound RF echoes which are predominantly independent of settings associated with the instrument and/or data acquisition session, with low levels of user dependency. Previous research conducted applying high-frequency (20–50 MHz) quantitative ultrasound to detect changes in tissue microstructure associated with cancer therapies using *in vitro*, *in situ*, and *in vivo* models have indicated its ability to detect cell death.[6–12] Initial observations demonstrated increased tissue echogenicity in cancer cells exposed to the chemotherapeutic agent cisplatinum.[6,7] Subsequent research used quantitative ultrasound spectroscopy in addition to statistical analysis of the ultrasound signal envelope to quantify this effect in a variety of *in vitro* and *in vivo* tumor models.[8,9] More recently, high-frequency ultrasound was used to detect apoptosis as an effect of photodynamic therapy, and effects of radiation therapy which induced apoptotic cell death in certain tumor models, and in other tumor models mitotic arrest.[10–12] Those studies indicated that high-frequency ultrasound is sensitive to structural changes associated with cell death with observed 16-fold maximal increases in backscatter signal intensity accompanied by changes in biomarkers including parameters such as spectral slope and 0-MHz intercept. These are quantitative ultrasound-based biomarkers which can be related to effective scatterer size and acoustic concentration, respectively.[13,14] Similar techniques have been employed previously in other quantitative ultrasound tissue characterization applications such as in the diagnoses of prostate cancer, liver, and cardiac abnormalities and the differentiation of benign fibroadenomas from mammary carcinomas and sarcomas.[15–17]

Although high-frequency ultrasound benefits from an increased imaging resolution (30–80 μm over 20–50 MHz) when compared to clinically utilized frequencies of (80 μm–1.5 mm resolution over 1–20 MHz), it suffers from limited tissue penetration depth constraining its use to superficial tissue sites. With greater tissue penetration, conventional-frequency ultrasound has the potential to noninvasively monitor the responses of patients undergoing therapies for a wide variety of deeper body cancers such as breast, kidney, and liver malignancies. The use of clinically relevant lower frequencies to detect changes in morphology in response to cell death induced by cancer treatment administration could thus permit assessing the effectiveness of an increased range of cancer therapies and guide their change from ineffective therapies to efficacious ones.

Investigations into the potential of low-frequency ultrasound in the detection of treatment response have been carried out using *in vitro* acute myeloid leukemia (AML) cell models. That work indicated that 10 MHz quantitative ultrasound spectroscopic analysis was able to quantify microstructural changes that are histologically correlated with apoptotic cell death in AML cells exposed to cisplatinum chemotherapy.[18] Time-dependant experiments indicated statistically significant changes in tissue characteristics within 6 h following drug administration. Additionally, concentration-dependent experimentation indicated the potential detection of as little as 2.5% apoptotic cells within an otherwise viable population sample.[18] Parallel data collection employing high-frequency ultrasound found favorable correlation in the detection of response across the employed frequency ranges via spectroscopic quantification of the normalized power spectrum. Other investigations also have indicated that the cell's nuclear configuration can have a significant influence on low and high-frequency ultrasound backscatter signal intensity.[12] We have previously demonstrated the ability of those biomarkers derived using high-frequency ultrasound to be used to track tumor responses to radiation.[10,11]

In this study, we have carried out assessments of tumor responses to different cancer treatments using conventional low-frequency (∼7 MHz) ultrasound biomarkers in order to demonstrate their potential to detect cell death. Concurrent confirmatory experiments were also performed using high-frequency (∼20 MHz) ultrasound data in order to further validate and support the results observed with the low-frequency data. The study here demonstrates for the first time the capacity of conventional-frequency ultrasound, in addition to high-frequency ultrasound, in quantifying apoptotic tumor cell death resulting from cancer therapy administration using preclinical *in vivo* models. Human breast cancer (MDA) and prostate cancer (PC3) bearing mice were treated with different cancer therapies. Breast (MDA) tumors were treated and evaluated after 0, 4, 12, and 24 h of chemotherapy (resulting in different levels of apoptosis). Prostate (PC3) tumors were exposed to no treatment, radiation alone (inducing mainly mitotic arrest), antivascular ultrasound therapy (inducing vascular disruption and consequently apoptotic cell death), as well as a combined treatment of the antivascular ultrasound therapy and radiation (producing more extensive apoptotic cell death).[19] Analysis of both low-frequency and corresponding high-frequency data used spectrum analysis in addition to statistical quantification of the signal envelope to derive ultrasound-based biomarkers. Results indicated that these biomarkers could be used to detect cell death induced by different types of treatments.

This study represents the first use of conventional-frequency ultrasound coupled with quantitative ultrasound-based biomarkers to noninvasively monitor cell death in response to cancer therapy *in vivo*. This work forms a basis for potentially using such biomarkers to monitor noninvasively cancer treatments in patients. In the future, it may be possible to guide the customization of cancer therapies by using such quantitative imaging techniques in order to change ineffective therapies to more efficacious treatments.

2. MATERIALS AND METHODS

2.A. Animal models

Experiments were conducted using xenografted human prostate (PC3) and breast (MDA-MB-231) tumors on hind legs of severe combined immunodeficiency disease (SCID) mice. Tumors reached a size of 7–9 mm at 4–5 weeks after injection of cells subcutaneously. Cell lines were obtained from American Type Culture Collection (ATCC, Manassas, VA). For imaging, mice were anesthetized (100 mg/kg ketamine, 5 mg/kg of xylazine, and 1 mg/kg of acepromazine, CDMV, St. Hyacinthe, Quebec, Canada) and the tumor and surrounding area were epilated before scanning (Nair™ Church & Dwight Co., Canada). Experimentation used 32 PC3 and 16 MDA bearing mice; each tumor type was divided equally into four treatment categories, one of which remained untreated as a control group (Table I).

2.B. Treatments

For the PC3 tumor model, the first treatment group was administered with vascular-targeting therapy consisting of a high-concentration dose (3% v/v; end microbubble volume relative to mouse blood volume) of ultrasonically stimulated microbubbles (Definity, Bristol-Myers Squibb, NY) to induce vascular disruption. The second group received an 8 Gy radiation using 160 kVp x-rays at 200 cGy/min (Faxitron Corporation, IL). The last group received a combination therapy consisting of the antivascular ultrasound and bubble therapy followed immediately by the x-ray radiation as above. Microbubble stimulation in these groups was carried out using an inhouse constructed system with an ultrasound excitation pulse centered at 500 kHz and a matched unfocussed transducer (Valpey Fisher, Hopkinton, MA) with a pulse repetition frequency of 3 kHz and peak negative pressure of 570 kPa

TABLE I. Number of animals in each treatment group. Control animals are untreated.

Tumor	Treatment			
PC3	Control	Antivascular microbubble + ultrasound	8 Gy radiation	Antivascular microbubble + ultrasound + 8 Gy radiation
	8	8	8	8
MDA	Control	4 h after chemotherapy exposure	12 h after chemotherapy exposure	24 h after chemotherapy exposure
	4	4	4	4

for a total administration time of 750 ms over a 5 min period in order to avoid any potential hyperthermic effects on tissue. This microbubble treatment alone causes vascular destruction leading to apoptosis and when combined with radiation yields rapid apoptotic cell death within the central core of these human xenograft tumors and is described elsewhere.[19]

The MDA tumor model was treated with Paclitaxel-Doxorubicin (150 mg/m^2, 50 mg/m^2) through an intravenous tail vein injection, to mimic human chemotherapy administration. Each MDA treatment group was assessed at a different time after chemotherapy exposure, i.e., 0, 4, 12, and 24 h, respectively. The purpose of the variation in the assessment time was to determine its effects on the tumor response and the sensitivity of quantitative ultrasound-based biomarkers to detect it.

2.C. Ultrasound data acquisition

Ultrasound data were collected from PC3 tumors prior to and 24 h following treatment, a time found to be optimal and potentially clinically relevant for response detection.[6–12] MDA tumors in each treatment group were imaged prior to therapy and at their group-specific time after chemotherapy exposure. Conventional-frequency ultrasound and RF data were acquired with a Sonix RP (Ultrasonix, Vancouver, Canada) system utilizing a L14-5/38 transducer with a transmit frequency of 10 MHz resulting in a frequency bandwidth with a center frequency of ~7 MHz, focused at 1.5 cm depth, and sampled at 40 MHz. High-frequency data were acquired with a Vevo 770 system (Visual Sonics, Toronto, Canada) using a transducer (RMV-710B) with a transmit frequency of 25 MHz resulting in a frequency bandwidth with a center frequency of ~20 MHz, and sampled at 420 MHz. Both systems were used to collect three-dimensional data with scan plane separations of 0.5 mm in the conventional-frequency data and 100 μm in the high-frequency data. Immediately following imaging animals were killed and tumors excised for histological examination.

2.D. Histological analyses

Histological analysis was carried out on tumor sections fixed in 5% formalin for 24–48 h and then sectioned in three representative planes with haematoxylin and eosin (H&E) staining carried out in addition to *in situ* end nick labeling (ISEL) and terminal deoxynucleotidyl transferase dUTP nick end labeling (TUNEL) immunohistochemistry for cell death. TUNEL is a sensitive method for detecting DNA fragmentation that results from apoptotic signaling cascades. Microscopy was carried out using a Leica DC100 microscope with a 20× objective and a Leica DC100 camera connected to a 2 GHz PC running Leica IM1000 software (Leica GmbH, Germany). Cell-death areas were quantified in histological immunohistochemistry tumor sections assisted by the use of Image-J (NIH, MD) macroscopically to detect TUNEL or ISEL positive areas in tumor sections. At higher magnifications (40×) apoptotic cells were counted manually by identifying typical apoptotic bodies. Similarly, quantification of cells undergoing mitotic arrest was performed by examination of four high magnification (40×) regions of H&E stained tumor sections per tumor, and manually determining the ratio of mitotically arrested cells to viable appearing tumor cells.

2.E. Ultrasound data analyses

Ultrasound data analysis was performed using the RF normalized power spectrum as well as statistical analysis of the signal envelope.[6–17,20] Representative data illustrating the general methods applied in this study are presented in Fig. 1. Figure 1 depicts ultrasound spectrum and histogram data along with parameters derived as ultrasound-based biomarkers and linked to histological cell death estimates.

Ultrasound data were analyzed across 10–15 individual equally spaced scan planes within a standardized region of interest (ROI) located at the tumor center which was consistently positioned at the transducer focal depth, accounting for approximately two third of the tumor area in cross-section plane (within the transducer's depth of field). The power spectrum was calculated using a Fourier transform of the raw radiofrequency data for each scan line through the ROI which was windowed using a Hamming function, and subsequently averaged. In order to remove effects of system transfer functions, data were normalized with a calibration pulse obtained from a flat quartz plate for high-frequency data.[13] Conventional-frequency data normalization employed the averaged power spectrum obtained at a 1.5 cm focal depth from an agar-embedded glass-bead phantom model[21,22] scanned with the same setting used for the tumor scans, in order to more accurately account for beam diffraction effects and other instrument-dependent factors, considering the use of a linear array transducer.

In order to calculate ultrasound-based spectroscopic biomarkers, linear regression analysis was performed on normalized power spectrum (in dBr), within a −6 dB window from the transducer center frequency determined from a calibration pulse (bandwidths of 4.5–9.0 and 13.5–27.5 MHz for low and high-frequency data, respectively), in order to generate a best-fit line (Fig. 1). Parameters determined included the midband fit (value of the fitted line at bandwidth center), the spectral slope (slope of the fitted line), and the corresponding 0-MHz intercept (interception of the fitted line with 0 MHz axis) (Refs. 23, 24, 14, and 20) which can be related to ultrasound backscatter power, effective scatterer size, and acoustic concentration, respectively.[13,14] By definition, any two out of these three parameters are independent, i.e., the third parameter can be derived from other two. All the parameters were determined for each of the 10–15 scan planes collected per specimen and averaged for each animal tumor in each treatment category. Parametric images of these ultrasound-based biomarkers were also generated for a visual representation of the RF data analysis by displaying the results of a sliding window analysis on a pixel by pixel basis within the ROI using a Hamming function. The parametric images were produced using a sliding window with a size of approximately 3 pulse lengths.

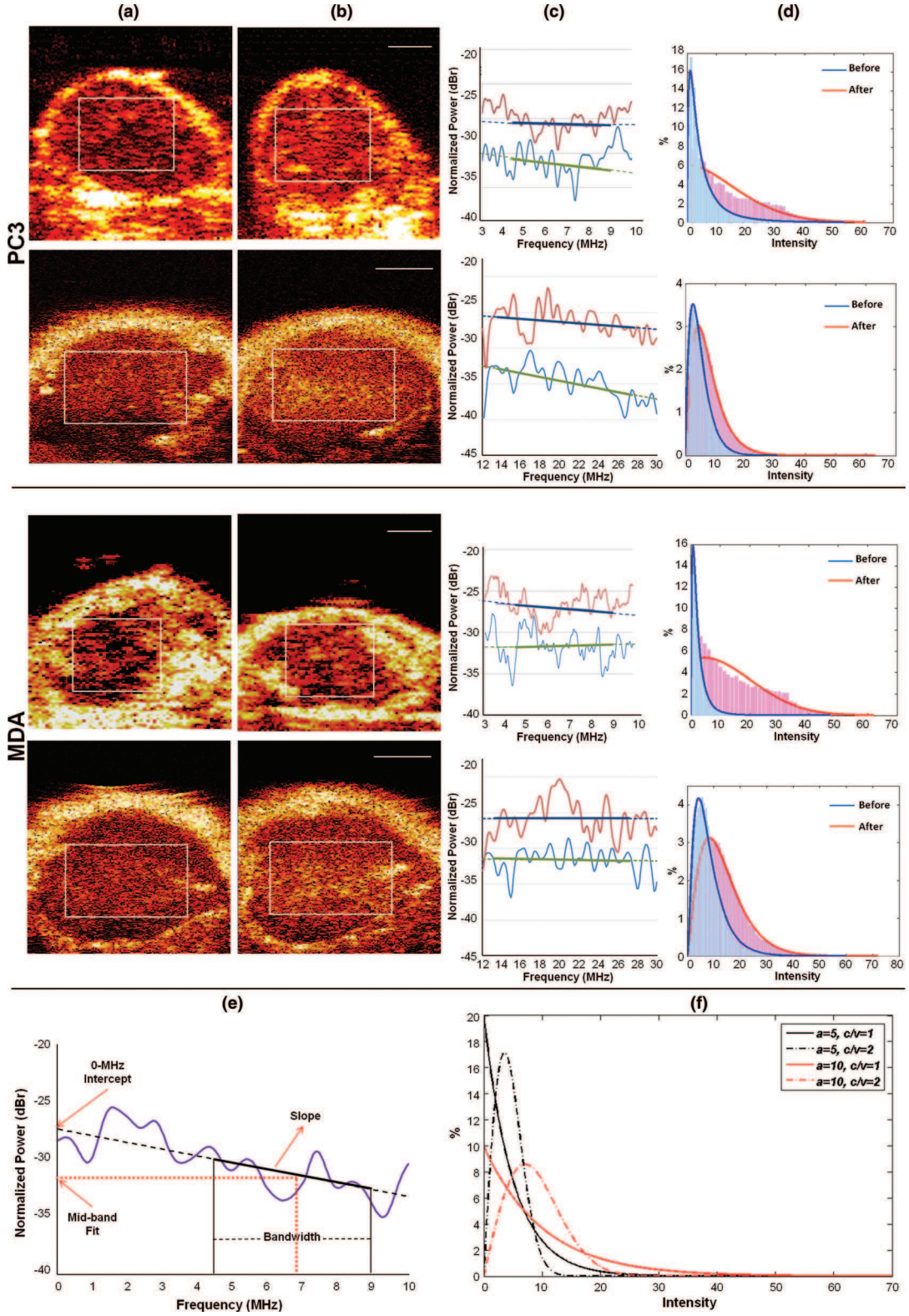

FIG. 1. Representative ultrasound-based biomarker data from PC3 and MDA tumors. Shown are a PC3 tumor treated with antivascular microbubble followed by 8 Gy x-rays and a chemotherapy treated MDA tumor both evaluated 24 h after exposure. (a) and (b) Representative ~7 MHz (first and third rows) and ~20 MHz (second and fourth rows) ultrasound B-mode images of untreated (a) and treated (b) tumors, demonstrating increases in tissue echogenicity with treatment compared to untreated tumor. ROIs applied in the quantitative analyses have been specified by rectangles. The scale bar represents ~3 mm. (c) Representative normalized power spectra obtained from tumors prior to treatment (blue) and afterwards (red). (d) Representative generalized gamma fitted histograms of the ultrasound signal intensity obtained from tumors prior to treatment and afterwards. (e) A schematic plot of the ultrasound normalized power spectrum demonstrating the extraction of spectroscopic biomarkers based on the linear regression analysis performed within −6 dB bandwidth. (f) A schematic plot of the generalized gamma distribution $[p(x) = \frac{cx^{cv-1}}{a^{cv}\Gamma(v)} e^{-(\frac{x}{a})^c}$, where Γ is the Gamma function, x is the signal intensity, a is the scale parameter, and c/v is the shape parameter], demonstrating effects of different histogram distributions of ultrasound signal intensity over two histogram-based biomarkers.

Statistical analysis of the signal envelope, another method to quantify ultrasound signals as response biomarkers,[8] used probability density function (PDF) histogram fitting as a way to perform envelope statistical parameter analysis.[25] Rayleigh and generalized gamma distributions were fitted to the histogram of the ultrasound signal envelope via maximum-likelihood estimation method, in order to obtain histogram-based biomarkers. The Rayleigh distribution σ parameter provided a biomarker indicative of ultrasound signal intensity.[26] The generalized gamma distribution parameters included shape (c/v) and scale (a) parameters which can be linked to the effective scatterer number density, and the effective scatterer cross-section, respectively.[8,27]

Tests of significance on changes in the quantitative ultrasound parameters were carried out using t-test (unpaired, two-sided, $\alpha = 0.05$) for both low-frequency and high-frequency data. Regression analyses (PASW Statistics 18, SPSS, Inc., Chicago, IL) were performed to evaluate correlations between changes in the quantitative ultrasound parameters, and percentage estimates of tumor cell-death obtained from histological analyses.

3. RESULTS

Representative ultrasound images and spectral data in addition to histogram-based data are presented in Fig. 1, demonstrating the calculation of the midband fit, 0-MHz intercept, and spectral slope as the spectroscopic biomarkers, in addition to the generalized gamma distribution shape and scale parameters as two histogram-based biomarkers applied in this study. Representative ultrasound-based biomarker results are presented for PC3 tumors treated with ultrasound-stimulated microbubbles in order to enhance radiation effects and for MDA tumors treated with chemotherapy. An overall increase in tissue echogenicity is visually detectable after treatment within responding tumor regions in both low-frequency and high-frequency ultrasound images. In these responding tumors, the presence of cell death was also reflected with changes in ultrasound spectra and histogram distribution of the ultrasound signal envelope for the treated tumors, which was quantified by the ultrasound-based biomarkers. Both treated tumor models exhibited cell death in gross morphological staining by TUNEL, ISEL, and H&E, and also at higher magnifications (described further below).

Changes in ultrasound-based biomarkers associated with treatment response are presented in Figs. 2–4. Results from conventional-frequency ultrasound are presented along with data from high-frequency ultrasound. The midband fit biomarker increased with treatments where there was prominent cell death noted histologically (Fig. 5). Mean increases in the midband fit biomarker of 0.1 ± 0.2, 3.4 ± 0.9, 4.8 ± 0.8, and 5.9 ± 0.9 dBr were observed for untreated, microbubble antivascular therapy, x-ray radiation, and combination therapy treatment groups of the PC3 tumor model [Fig. 2(a)]. These data paralleled results observed for high-frequency data for the same treatment groups, respectively. A similar trend was also obtained for the MDA tumor model treated with chemotherapy.

The spectral slope biomarker also demonstrated changes increasing with treatments that induced progressively more cell death, but showed the opposite change with chemotherapy-related cell death in MDA tumors [Fig. 2(b)]. The results associated with PC3 tumors proved to be statistically significant with $p < 0.05$ in both high and low-frequency treated data when compared to untreated animals, with the exception of the 8 Gy treatment set which exhibited a higher standard deviation when compared to the remaining treatment groups. For the MDA tumors, the spectral slope decreased in most cases in response to the chemotherapy, but was not statistically significant when compared to untreated animals.

The 0-MHz intercept biomarker demonstrated increases with treatments that induced progressively more cell death. For this parameter, changes of -0.3 ± 0.6, 2.9 ± 0.7, 4.1 ± 0.9, and 4.8 ± 1.2 dBr were observed for the control, microbubble antivascular therapy, x-ray radiation, and combination therapy groups of PC3 tumors, respectively [Fig. 2(c)]. It indicated peak changes in chemotherapy data (MDA tumors) at 24 h after treatment consistent with the changes in the other two ultrasound-based biomarkers.

The histogram-based biomarkers revealed general trends similar to the spectrum derived biomarkers (Fig. 3). However, compared to the low-frequency data, high-frequency results for the generalized gamma shape and scale parameters indicated smaller increases in the parameters with the treatments.

Data from low-frequency ultrasound and high-frequency ultrasound were consistent in terms of general trends exhibited in ultrasound-based biomarkers with different treatments. Data compared to untreated samples were statistically significant except for the spectral slope and generalized gamma shape parameters in the chemotherapy experiments which exhibited greater variability than the other biomarkers.

Figure 4 demonstrates representative ultrasound B-mode images with parametric overlays of the 0-MHz intercept biomarker for different treatments, demonstrating the use of quantitative ultrasound parameters to discriminate differences in response between groups and depicting the potential of this technique to identify response heterogeneity.

Histology and cell-death immunohistochemistry associated with treatments is presented in Fig. 5. It indicated small amounts of cell death associated with treatments with radiation or ultrasound-stimulated microbubbles alone. Large regions of cell death in combined treatments were apparent with a diminishment in nuclear size associated with apoptotic cell death evident in higher-magnification histology. In treatments with chemotherapy, increases in cell death were apparent with the treatment groups assessed at longer times after chemotherapy exposure. High magnification histology indicated the presence of nuclear condensation progressing with time, with apoptotic features present at 24 h in the form of nuclear pyknosis and apoptotic bodies.

In PC3 tumors, histological analyses resulted in $1 \pm 1\%$, $8 \pm 2\%$, $17 \pm 7\%$, and $50 \pm 12\%$ mean ratios ($\pm$ standard error) of cell death within the control, microbubble antivascular therapy, x-ray radiation, and combination therapy groups, respectively. Although PC3 tumors treated with x-rays alone did not undergo significant amounts of apoptotic

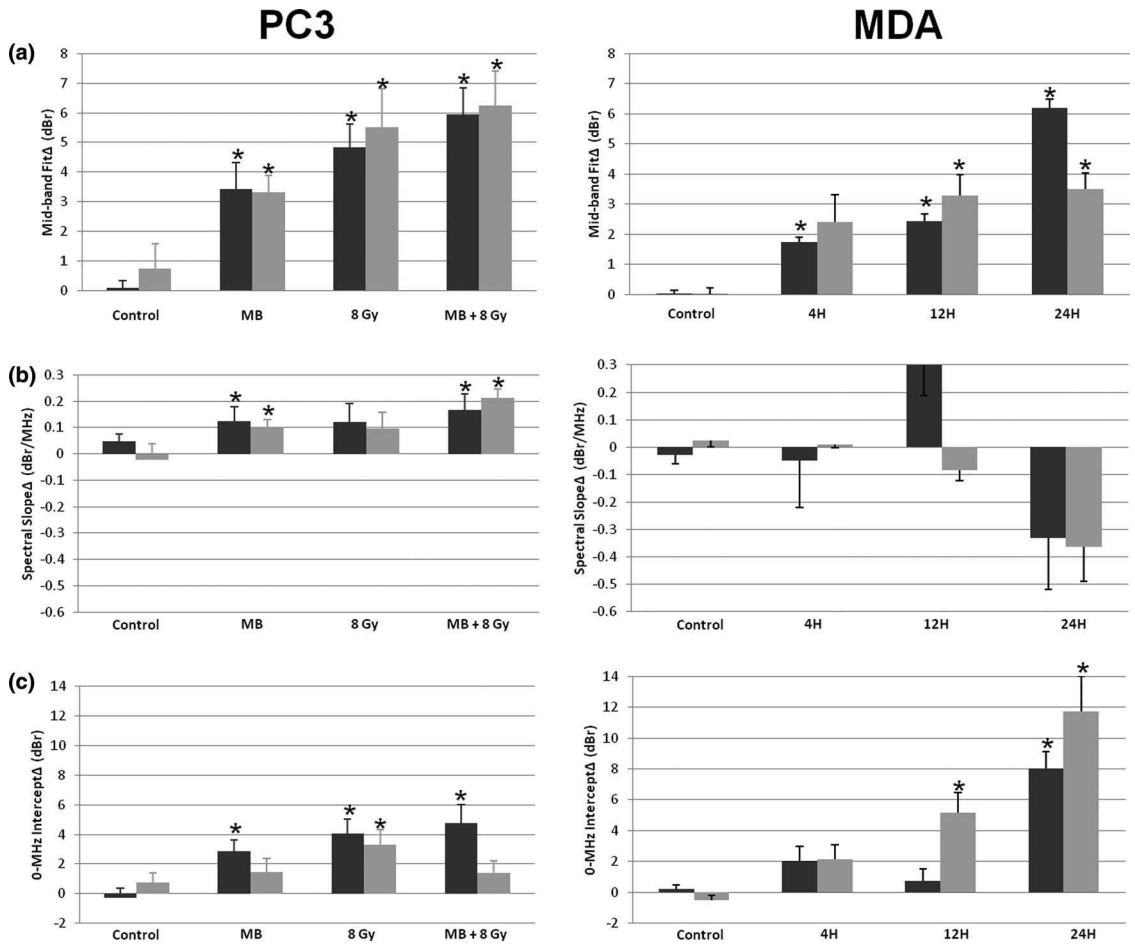

FIG. 2. Changes in the midband fit (a), spectral slope (b), and 0-MHz intercept (c) biomarkers for high and low-frequency data in the eight treatment groups of PC3 and MDA tumors. Control animals are untreated, MB indicates antivascular microbubble and ultrasound treatment animals, 8 Gy represents radiation treatments alone, MB + 8 Gy represents the combined treatment groups. 4, 12, and 24 h represent different times of evaluation after chemotherapy exposure. Dark and light bars represent low and high-frequency data, respectively. Error bars represent ± one standard error. Stars represent statistically significant differences ($p < 0.05$) in comparison to the control.

cell death, high magnification analysis of haematoxylin-and-eosin stained tumor sections indicated that significant portions of the x-ray treated tumors demonstrated significant changes in morphology when compared to the untreated specimens with prominent mitotic arrest/catastrophe and cellular and nuclear irregularities such as cellular swelling and multinucleated cells consistent with mitotic death. In MDA tumors, immunohistochemistry staining for cell death revealed 8 ± 2%, 20 ± 7%, 22 ± 5%, and 61 ± 12% mean areas (± standard error) of apoptotic cell death within the groups evaluated at 0, 4, 12, and 24 h after chemotherapy exposure, respectively.

Linear regression analyses performed to assess correlations between changes in the conventional-frequency midband fit biomarker and the percentage estimates of histological tumor cell-death resulted in r^2 values of 0.71 and 0.82 ($p < 0.001$) for PC3 and MDA tumors, respectively (Fig. 6). This indicates a strong correlation between obtained spectroscopic results, and the corresponding tumor responses to treatment observed histologically. Quadratic regression analyses performed to assess levels of nonlinearity resulted in slightly improved r^2 values of 0.76 and 0.84 ($p < 0.001$) for PC3 and MDA tumors, respectively (Fig. 6).

4. DISCUSSION

The results demonstrate for the first time that clinically relevant conventional-frequency ultrasound may be used to detect cell death *in vivo* in well controlled preclinical animal models exhibiting cell death. Compared to untreated control animals ultrasound-based spectroscopic response biomarkers (utilizing midband fit, spectral slope and 0-MHz intercept parameters) and histogram-based biomarkers (including Rayleigh σ parameter and generalized gamma shape and scale parameters) indicated consistent changes associated with histological increases in cell death. Histological analyses indicated that a mix of mitotic arrest/catastrophe leading to apoptotic death was induced by 8 Gy treatments, whereas apoptotic cell death was induced by antivascular treatment secondary to vascular disruption.[19] Greater amounts of apoptotic death were observed in combination treatments, as well as in the treatment groups assessed at longer times after chemotherapy exposure. We have demonstrated the detection in such cell-death models using high-frequency ultrasound before,[10–12] but here for the first time at low and more clinically relevant frequencies. Changes in ultrasound-based

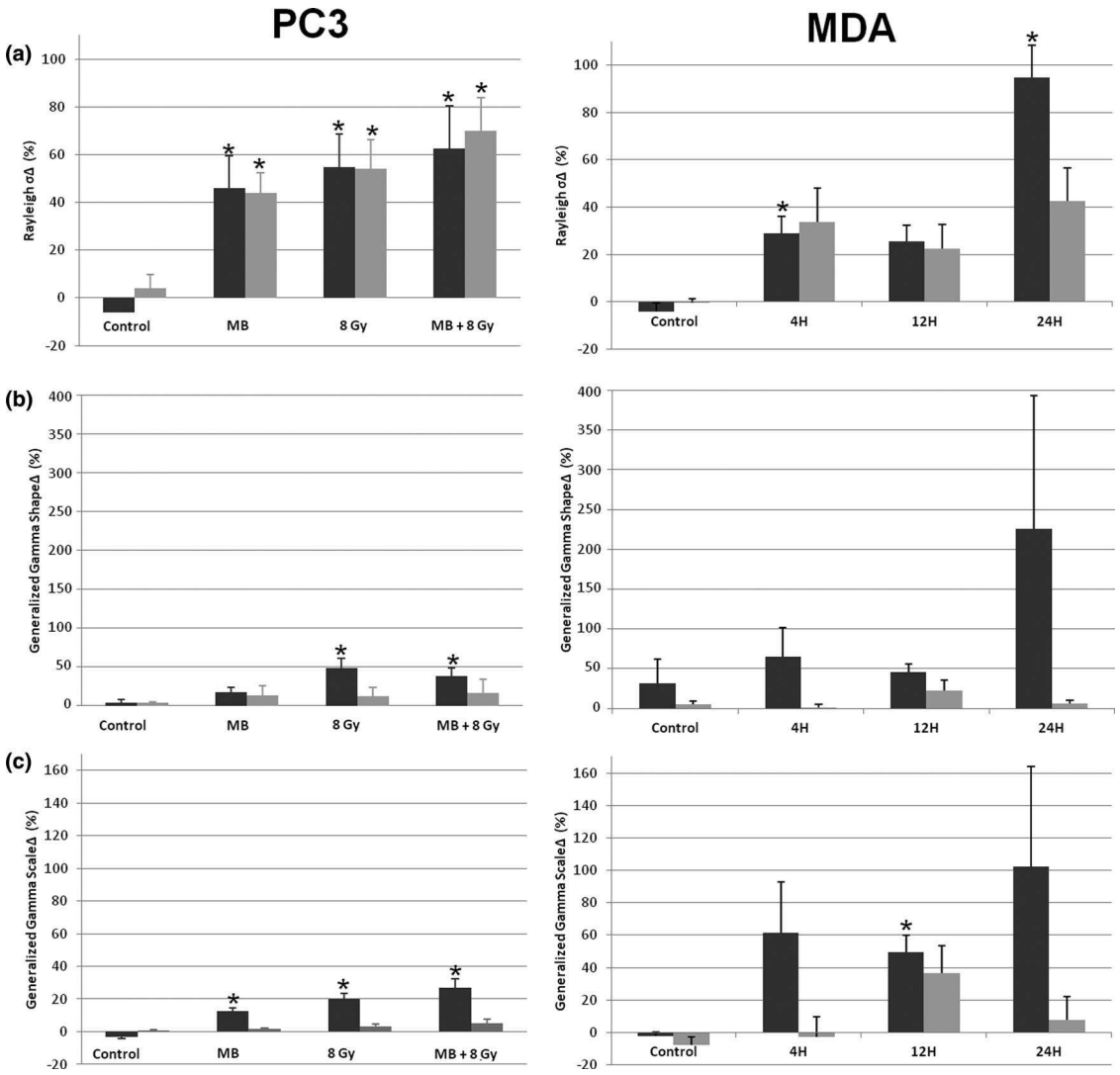

FIG. 3. Percentage changes in the Rayleigh σ parameter (a), generalized gamma shape parameter (b), and generalized gamma scale parameter (c) for high and low-frequency data in the eight treatment groups of PC3 and MDA tumors. Control animals are untreated, MB indicates antivascular microbubble and ultrasound treatment animals, 8 Gy represents radiation treatments alone, MB + 8 Gy represents the combined treatment groups. 4, 12, and 24 h represent different times of evaluation after chemotherapy exposure. Dark and light bars represent low and high-frequency data, respectively. Error bars represent ± one standard error. Stars represent statistically significant differences ($p < 0.05$) in comparison to the control.

spectroscopic biomarkers with different treatments were apparent and samples which displayed macroscopic areas of cell death demonstrated changes in low and high-frequency ultrasound data. The midband fit biomarker increases ranged approximately from 0 to 6 dBr for samples concordant with increases in cell death apparent histologically. Correlations estimated via linear regression analyses between changes in the midband fit biomarker and histological estimates of cell death resulted in $r^2 = 0.71$ and $r^2 = 0.82$ for PC3 and MDA tumors, respectively, and was statistically significant for both with $p < 0.001$.

Data obtained from PC3 tumors indicated coincident increases in trend for the spectral slope biomarker from high and low-frequency data. Here, observed increases with different treatment types are consistent with the interpretation of scatterer sizes becoming smaller as observed in histological morphology with nuclear condensation and fragmentation. Spectral data obtained in this study from MDA tumors, however, demonstrated decreases in the spectral slope biomarker for high and low-frequency data, in most cases. This may be related to the development of patches of response in larger structures of scatterers such as glands, in MDA human breast tumors. Development of such larger structures is less likely expected in the case of PC3 human prostate tumors which are highly cellular small-cell-like tumors with little higher-order organization.

Previous studies using 10–40 MHz ultrasound frequencies have demonstrated that isolated nuclei from apoptotic cells exhibited increases in backscatter signal intensity compared to nuclei from viable cells, which were consistent with changes in cells undergoing apoptosis.[12] In the study here, increases in the 0-MHz intercept biomarker also occurred with the combined treatments in PC3 tumors in which this was less apparent with high-frequency ultrasound. We suspect that the

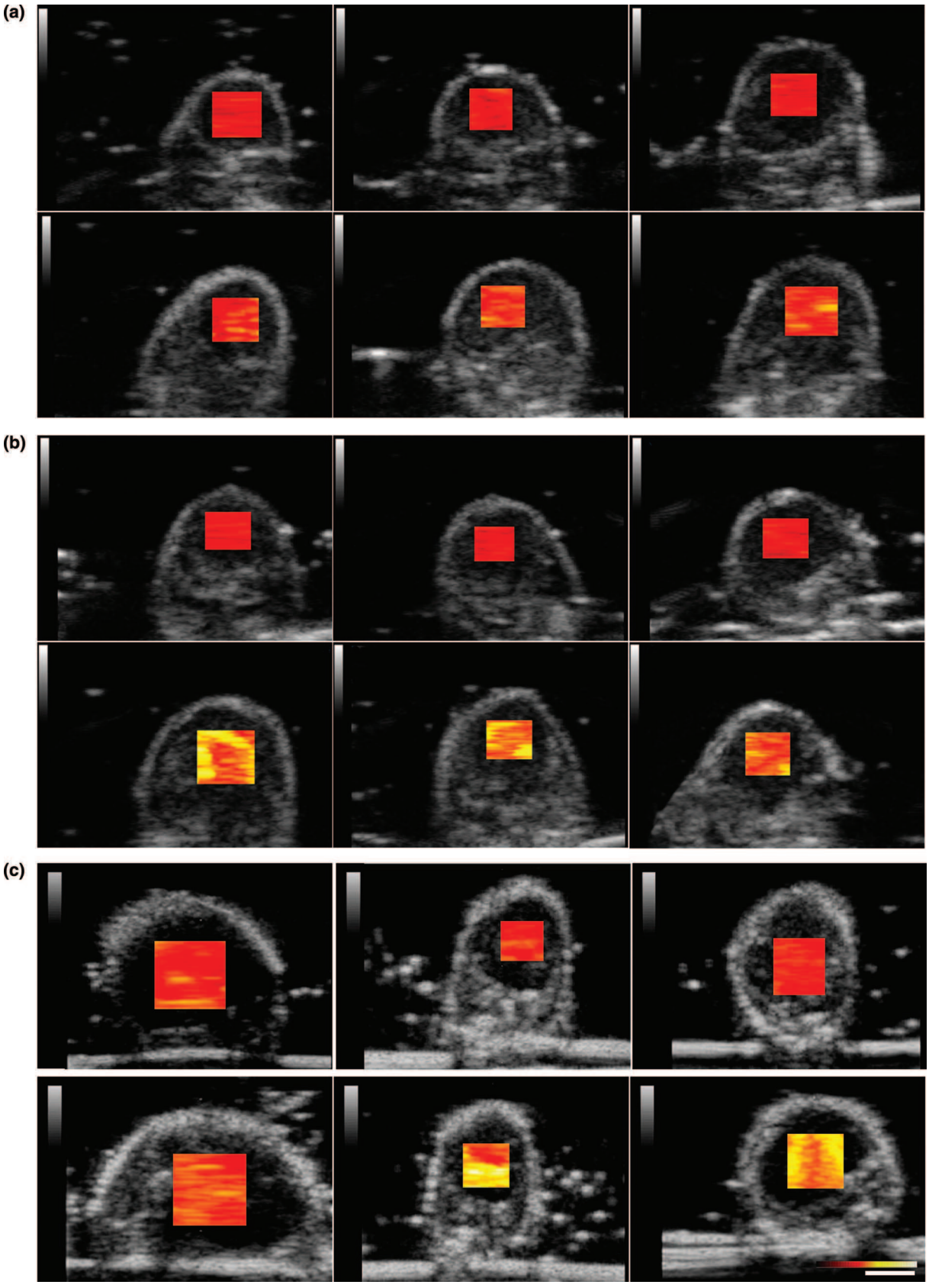

FIG. 4. Low-frequency ultrasound B-mode images with ROI parametric overlays of the 0-MHz intercept biomarker for (a): PC3 tumors treated with antivascular microbubble therapy, (b): PC3 tumors treated with antivascular microbubble followed by 8 Gy x-ray treatment, and (c) MDA tumors were treated and evaluated at 4 (left), 12 (middle), and 24 (right) h after chemotherapy exposure. The topmost rows of images consist of data acquired prior to treatment, and the bottom following respective treatments. Scale bars represent ~5 mm. The color bar represents a scale encompassing ~100 dBr. The color bar scale were kept consistent covering the dynamic range observed in all the treatment groups before and after the treatment, in order to enable valid intergroup comparisons.

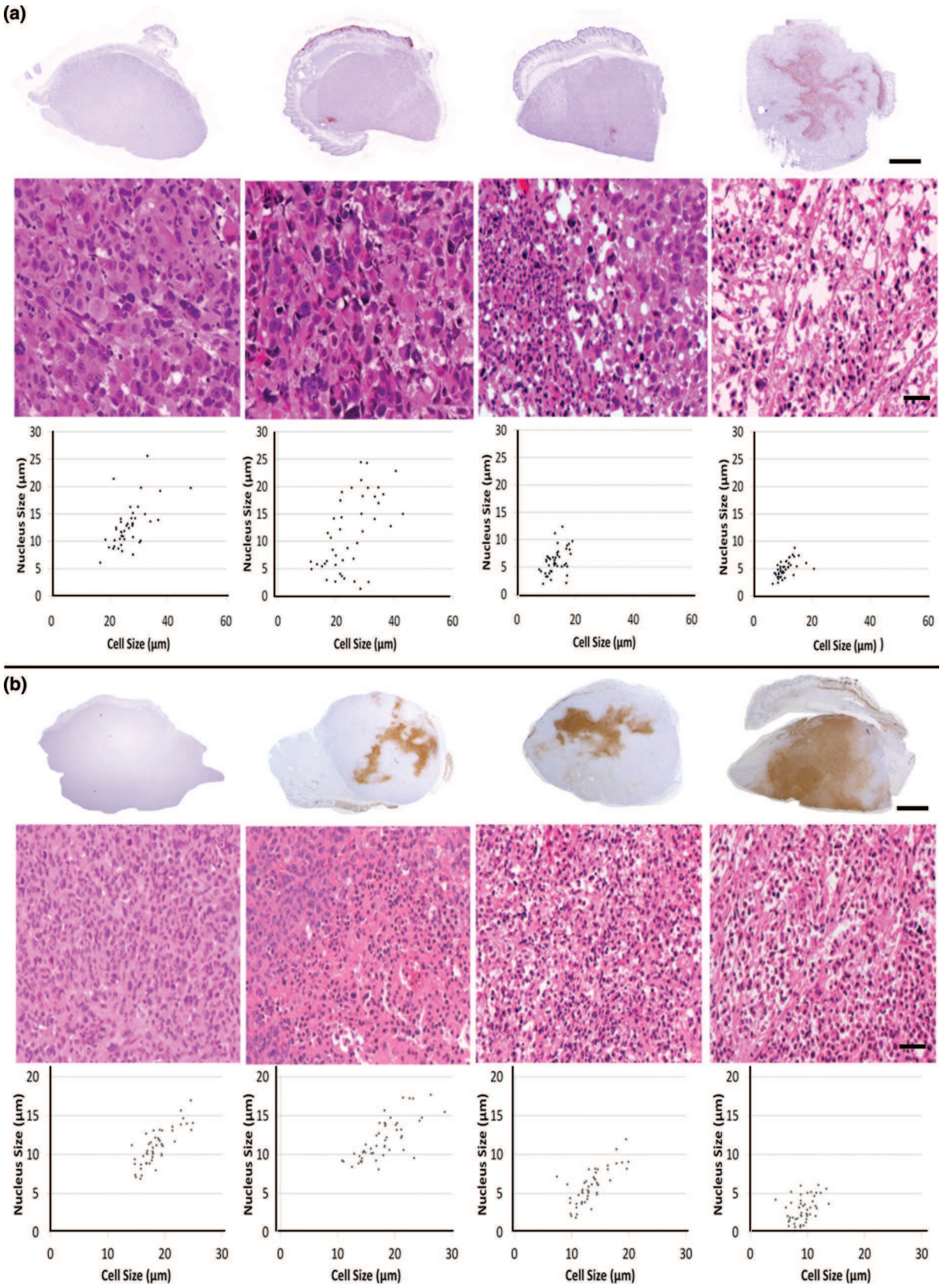

FIG. 5. (a) Representative data from untreated, anti-vascular microbubble, 8 Gy x-ray, and antivascular microbubble followed by 8 Gy x-ray treatment groups of PC3 tumors, from left to right, respectively. (b) Representative data from untreated group, as well as the treatment groups of MDA tumors evaluated at 4, 12, and 24 h after chemotherapy exposure of, from left to right, respectively. (First row) Low-magnification light microscopy images of TUNEL (PC3) and ISEL (MDA) stained tumors, demonstrating the areas of apoptotic cell death. The scale bar represents ~2 mm. (Second row) Light microscopy images of haematoxylin and eosin stained tumor slices obtained at high magnification. The scale bar represents ~10 (PC3) and ~50 (MDA) μm. (Third row) Distribution of cell versus nucleus size measurements representing morphology of responsive regions within the tumor.

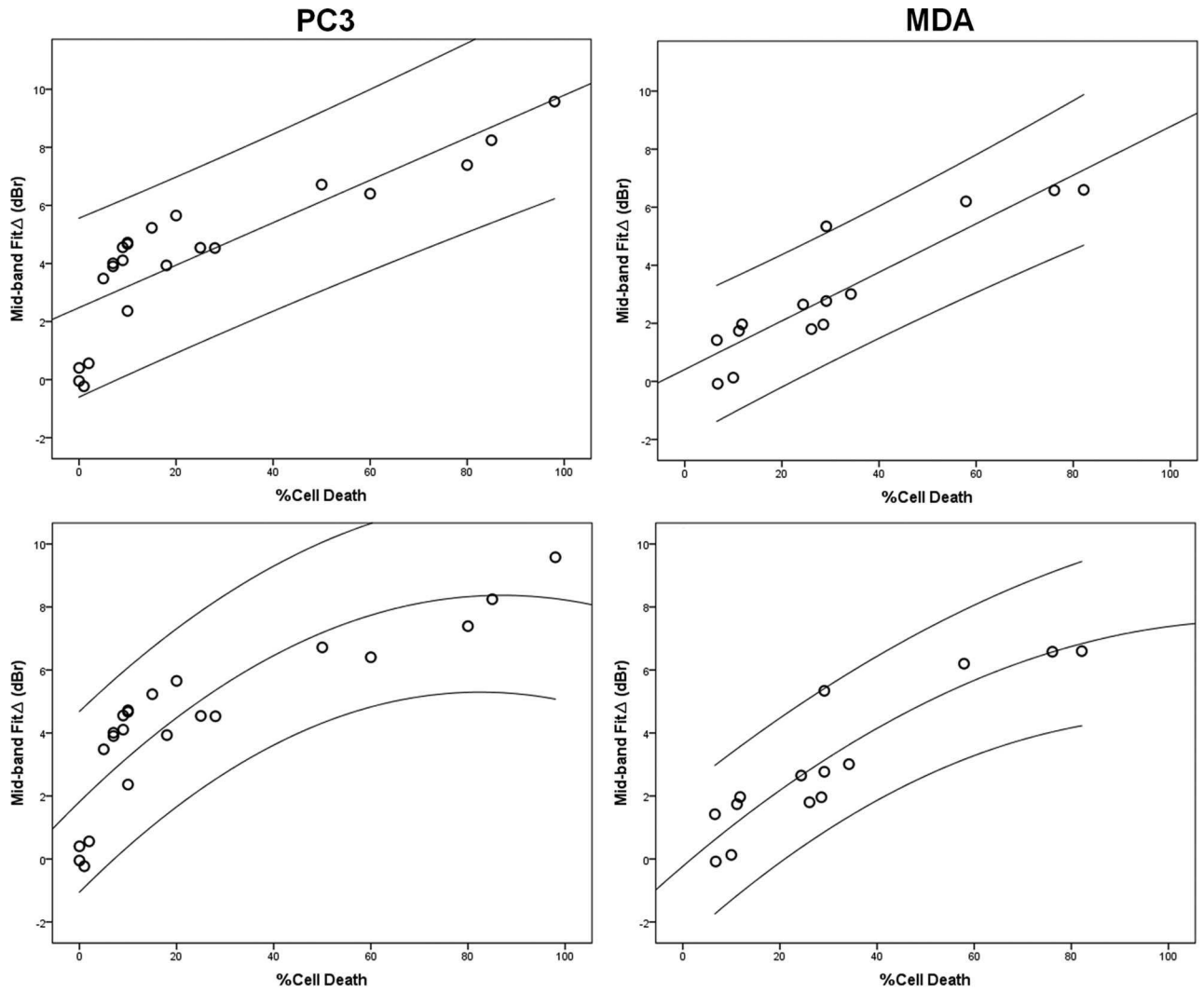

FIG. 6. Results of linear (first row) and quadratic (second row) regression analyses performed on the percentages of histological cell death and changes in the midband fit biomarker after treatment administration, within the 95% confidence interval. Data represent the results obtained from PC3 and MDA tumors of different treatment groups. The linear analyses resulted in r^2 values of 0.71 and 0.82 ($p < 0.001$) for PC3 and MDA tumors, respectively. The quadratic analyses resulted in r^2 values of 0.76 and 0.84 ($p < 0.001$) for PC3 and MDA tumors, respectively.

nuclear degeneration and disintegration (necrosis) which was most prominent in these samples has a greater effect upon high-frequency data than low-frequency data, with predominant loss of cell structure leading to a less prominent increase in this parameter. Advanced necrosis has been demonstrated by others to result in decreases in backscatter intensity.[28] In the results associated with MDA tumors, the largest increases in the 0-MHz intercept biomarker occurred with the longest assessment time after the chemotherapy exposure (24 h) for high and low-frequency data, since the chemotherapy alone would less likely result in progressed cell death earlier than 24 h of exposure. Results from histogram-based biomarkers followed the same general trends indicated by spectroscopic biomarkers. These measures have been used before with cells treated with chemotherapy, but only with high-frequency ultrasound and are explained in depth elsewhere.[8]

The results in this study are supported by previous investigations of cell-death detection *in vitro* and *in vivo* using high-frequency ultrasound.[6–12] Those studies indicated an important role of nuclear structure in which induced nuclear condensation either by the induction of mitotic death or apoptotic death can lead to increases in backscatter signal intensity. Other research comparing low-frequency and high-frequency data predominantly from *in vitro* cell models has indicated a correspondence such as that seen here for experiments done following cell-death progression with time and extent of cell death.[18] Samples here demonstrated increases in cell death and had consequent changes in ultrasound-based response biomarkers which followed trends of increases in cell death in histologically analyzed samples. The fact that the low-frequency data were mirrored in trend by the high-frequency data was reassuring, although the nature of the scatterers expected from the two samples is potentially different. We would expect Rayleigh scattering (backscatter intensity proportional to f^4, where f is frequency) (Ref. 29) to predominate at low frequencies as the cellular components are significantly smaller than the ultrasound wavelengths, whereas with high-frequency ultrasound cellular components are

approximately of the same order as the ultrasound wavelength (with a more complex relationship between backscatter intensity and frequency). Our "working" hypothesis is that the condensation of nuclear structure during cell death (pyknosis, karyorrhexis) results in an increased ultrasound backscatter signal intensity.

There are now multiple sources of experimental evidence suggesting a role for nuclear structure in contributing to ultrasound backscatter signals.[12] This evidence includes:

(1) In highly cellular xenograft tumors, backscatter signals and spectra are identical to backscatter signals and spectra of centrifuged cell models that mimic the histological packing of xenograft tumors.[30,31] Such packed cell models have no extracellular matrix and collagen present yet exhibit nearly identical backscatter profiles.
(2) Different cell types may be differentiated on the basis of their ultrasound spectra, now recognized to be linked to nuclear size in such a manner. This has further suggested to us an important role of nuclear structure in ultrasound backscatter signal.[32]
(3) In cell experiments where nuclear structure is specifically modified, there are changes in ultrasound backscatter signal. Treatment of cells with colchicine to arrest them in G2/M of mitosis with condensed nuclear material demonstrated significant increases in ultrasound backscatter and such increases were reversed by digesting cellular DNA through enzymatically treating such colchicine treated cells with DNAse.[7] Other changes induced by sodium butyrate causing unfolding of nuclear structure demonstrate decreases in ultrasound backscatter.[33] And,
(4) Calculated scatterer sizes from ultrasound backscatter do not work out to be the same as cell sizes but coincide with smaller sizes near that of nuclei suggestive again of an important role of the nucleus.[30,31]

One may not expect at ~7 MHz there to be sizeable ultrasound backscatter changes from micrometer-sized particles mainly due to loss of scattering strength of small scattering structures. However, in this low- to mid-frequency range (near 10 MHz), we believe that bulk changes in tissue are related to ensembles of cells and nuclei smaller than the wavelength of the ultrasound being used. These ensembles influence acoustic properties and thus ultrasound backscatter properties. As discussed earlier, the potential scatterers are closer in size to those that predominate in the Rayleigh scattering regime, as they are about ten times smaller than the interrogating wavelength (10–30 versus 100–300 μm). When imaging cell samples, even at these low frequencies, a speckle pattern is still formed indicating that many subresolution scatterers contribute to detected signals. At ultrasound high frequencies, the spatial organization of cellular-based scatterers can also influence ultrasound backscatter properties and this can also be a factor at low frequencies.[34]

The work here complements other noninvasive imaging methods such as those based on positron emission tomography or magnetic resonance imaging being investigated to detect tumor responses.[1,2,35,36] Different from these methods, our ultrasound method relies on inherent contrast changes arising from changes in acoustic properties as cancer cells die. The preclinical work here applied in xenograft models appears to be able to be extrapolated to human data for response monitoring[37–39] at depth.

In conclusion, this study indicates for the first time that low-frequency quantitative ultrasound techniques may be used to detect cell death *in vivo* and is supported by corresponding high-frequency ultrasound data. Ultrasound-based response biomarkers were obtained for four different manners of inducing cell death in preclinical prostate and breast cancer xenografts and analyses indicated a concordance between changes in ultrasound-based biomarkers and the histological extent of cell death. As such, this work forms the basis for the application of such low-frequency approaches *in vivo* in cancer patients for the monitoring and customization of their cancer therapies.

ACKNOWLEDGMENTS

A.S.N. holds a Banting Postdoctoral Fellowship, and also held a Canadian Breast Cancer Foundation Postdoctoral Fellowship partly during the conduct of this research. O.F. holds a Canadian Breast Cancer Foundation Postdoctoral Fellowship. H.T. holds a Natural Sciences and Engineering Research Council of Canada Alexander Graham Bell Graduate Scholarship. G.J.C. holds a Cancer Care Ontario Research Chair in experimental therapeutics and imaging. This study was funded, in part, by the Canadian Breast Cancer Foundation—Ontario Region. Funding for this project was also provided by the Terry Fox Foundation, the Natural Sciences and Engineering Research Council of Canada, and the Canadian Institutes of Health Research. The authors thank William Tran for assisting with the experiments.

[a]Author to whom correspondence should be addressed. Electronic mail: Gregory.Czarnota@sunnybrook.ca; Telephone: 416-480-6100 ext. 7073; Fax: 416-480-6002.

[1]K. Brindle, "New approaches for imaging tumour responses to treatment," Nat. Rev. Cancer **8**(2), 94–107 (2008).
[2]A. Sadeghi-Naini *et al.*, "Imaging innovations for cancer therapy response monitoring," Imaging Med. **4**(3), 311–327 (2012).
[3]O. Falou, A. Sadeghi-Naini, H. Soliman, M. J. Yaffe, and G. J. Czarnota, "Diffuse optical imaging for monitoring treatment response in breast cancer patients," in *Proceedings of the 34th Annual International Conference of the IEEE Engineering in Medicine and Biology Society (EMBC), San Diego, CA, 2012* (IEEE, Washington, DC, 2012), pp. 3155–3158.
[4]O. Falou *et al.*, "Diffuse optical spectroscopy evaluation of treatment response in women with locally advanced breast cancer receiving neoadjuvant chemotherapy," Transl. Oncol. **5**(4), 238–246 (2012).
[5]O. Falou *et al.*, "Evaluation of neoadjuvant chemotherapy response in women with locally advanced breast cancer using ultrasound elastography," Transl. Oncol. **6**(1), 17–24 (2013).
[6]G. J. Czarnota *et al.*, "Ultrasonic biomicroscopy of viable, dead and apoptotic cells," Ultrasound Med. Biol. **23**(6), 961–965 (1997).
[7]G. J. Czarnota *et al.*, "Ultrasound imaging of apoptosis: High-resolution non-invasive monitoring of programmed cell death *in vitro*, *in situ* and *in vivo*," Br. J. Cancer **81**(3), 520–752 (1999).
[8]A. S. Tunis, G. J. Czarnota, A. Giles, M. D. Sherar, J. W. Hunt, and M. C. Kolios, "Monitoring structural changes in cells with high-frequency

ultrasound signal statistics," Ultrasound Med. Biol. **31**(8), 1041—1049 (2005).
[9]M. C. Kolios, G. J. Czarnota, M. Hussain, F. S. Foster, J. W. Hunt, and M. D. Sherar, "Analysis of ultrasound backscatter from ensembles of cells and isolated nuclei," in *Proceedings of IEEE Ultrasonics Symposium, Atlanta, GA, 2001* (IEEE, Washington, DC, 2001), pp. 1257–1260.
[10]R. M. Vlad, N. M. Alajez, A. Giles, M. C. Kolios, and G. J. Czarnota, "Quantitative ultrasound characterization of cancer radiotherapy effects *in vitro*," Int. J. Radiat. Oncol., Biol., Phys. **72**(4), 1236–1243 (2008).
[11]R. M. Vlad, S. Brand, A. Giles, M. C. Kolios, and G. J. Czarnota, "Quantitative ultrasound characterization of responses to radiotherapy in cancer mouse models," Clin. Cancer Res. **15**(6), 2067–2075 (2009).
[12]B. Banihashemi, R. Vlad, B. Debeljevic, A. Giles, M. C. Kolios, and G. J. Czarnota, "Ultrasound imaging of apoptosis in tumor response: Novel preclinical monitoring of photodynamic therapy effects," Cancer Res. **68**(20), 8590–8596 (2008).
[13]F. L. Lizzi, M. Ostromogilsky, E. J. Feleppa, M. C. Rorke, and M. M. Yaremko, "Relationship of ultrasonic spectral parameters to features of tissue microstructure," IEEE Trans. Ultrason. Ferroelectr. Freq. Control **34**(3), 319–329 (1987).
[14]F. L. Lizzi, M. Astor, T. Liu, C. Deng, D. J. Coleman, and R. H. Silverman, "Ultrasonic spectrum analysis for tissue assays and therapy evaluation," Int. J. Imaging Syst. Technol. **8**(1), 3–10 (1997).
[15]M. L. Oelze, W. D. O'Brien, J. P. Blue, and J. F. Zachary, "Differentiation and characterization of rat mammary fibroadenomas and 4T1 mouse carcinomas using quantitative ultrasound imaging," IEEE Trans. Med. Imaging **23**(6), 764–771 (2004).
[16]E. J. Feleppa *et al.*, "Typing of prostate tissue by ultrasonic spectrum analysis," IEEE Trans. Ultrason. Ferroelectr. Freq. Control **43**(4), 609–619 (1996).
[17]M. Yang, T. M. Krueger, J. G. Miller, and M. R. Holland, "Characterization of anisotropic myocardial backscatter using spectral slope, intercept and midband fit parameters," Ultrason. Imaging **29**(2), 122–134 (2007).
[18]M. Azrif, S. Ranieri, A. Giles, B. Debeljevic, M. C. Kolios, and G. J. Czarnota, "Conventional low-frequency ultrasound detection of apoptosis," in *Proceedings of American Institute of Ultrasound in Medicine Annual Convention, New York, NY, 2007* (AIUM, Laurel, MD, 2007), p. S185.
[19]G. J. Czarnota *et al.*, "Tumor radiation response enhancement by acoustical stimulation of the vasculature," Proc. Natl. Acad. Sci. U.S.A. **109**(30), E2033–E2041 (2012).
[20]F. L. Lizzi, M. Greenebaum, E. J. Feleppa, M. Elbaum, and D. J. Coleman, "Theoretical framework for spectrum analysis in ultrasonic tissue characterization," J. Acoust. Soc. Am. **73**(4), 1366–1373 (1983).
[21]L. X. Yao, J. A. Zagzebski, and E. L. Madsen, "Backscatter coefficient measurements using a reference phantom to extract depth-dependent instrumentation factors," Ultrason. Imaging **12**(1), 58–70 (1990).
[22]F. Dong, E. L. Madsen, M. C. MacDonald, and J. A. Zagzebski, "Nonlinearity parameter for tissue-mimicking materials," Ultrasound Med. Biol. **25**(5), 831–838 (1999).
[23]E. J. Feleppa, F. L. Lizzi, D. J. Coleman, and M. M. Yaremko, "Diagnostic spectrum analysis in ophthalmology: A physical perspective," Ultrasound Med. Biol. **12**(8), 623–631 (1986).
[24]M. L. Oelze and W. D. O'Brien, "Method of improved scatterer size estimation and application to parametric imaging using ultrasound," J. Acoust. Soc. Am. **112**(6), 3053–3063 (2002).
[25]D. W. Scott, "On optimal and data-based histograms," Biometrika **66**(3), 605–610 (1979).
[26]R. C. Molthen *et al.*, "Comparisons of the Rayleigh and K-distribution models using *in vivo* breast and liver tissue," Ultrasound Med. Biol. **24**(1), 93–100 (1998).
[27]A. S. Tunis, "Monitoring structural changes in cells and tissues with high frequency ultrasound signal statistics," M.Sc. Thesis, University of Toronto, 2005.
[28]V. Rouffiac *et al.*, "Validation of a new method for quantifying *in vivo* murine tumor necrosis by sonography," Invest. Radiol. **39**(6), 350–356 (2004).
[29]J. W. Strutt, "Investigation of the disturbance produced by a spherical obstacle on the waves of sound," Proc. London Math. Soc. **s1–s4**(1), 253–283 (1871).
[30]R. M. Vlad, "Quantitative ultrasound chacterization of responses to radiotherapy *in vitro* and *in vivo*," Ph.D. Thesis, University of Toronto, 2009.
[31]M. L. Oelze and W. D. O'Brien, "Application of three scattering models to characterization of solid tumors in mice," Ultrason. Imaging **28**(2), 83–96 (2006).
[32]L. R. Taggart, R. E. Baddour, A. Giles, G. J. Czarnota, and M. C. Kolios, "Ultrasonic characterization of whole cells and isolated nuclei," Ultrasound Med. Biol. **33**(3), 389–401 (2007).
[33]G. J. Czarnota and M. C. Kolios, "Ultrasound imaging of apoptosis: Role of chromatin structure and membrane configuration," in *Proceedings of American Institute of Ultrasound in Medicine Annual Convention, Orlando, FL*, 2001 (AIUM, Laurel, MD, 2001), p. S117.
[34]J. W. Hunt, A. E. Worthington, A. Xuan, M. C. Kolios, G. J. Czarnota, and M. D. Sherar, "A model based upon pseudo regular spacing of cells combined with the randomisation of the nuclei can explain the significant changes in high-frequency ultrasound signals during apoptosis," Ultrasound Med. Biol. **28**(2), 217–226 (2002).
[35]T. H. Witney and K. M. Brindle, "Imaging tumour cell metabolism using hyperpolarized 13C magnetic resonance spectroscopy," Biochem. Soc. Trans. **38**(5), 1220–1224 (2010).
[36]T. H. Witney *et al.*, "Detecting treatment response in a model of human breast adenocarcinoma using hyperpolarised [1-^{13}C]pyruvate and [1,4-$^{13}C_2$]fumarate," Br. J. Cancer **103**(9), 1400–1406 (2010).
[37]A. Sadeghi-Naini *et al.*, "Quantitative ultrasound evaluation of tumour cell death response in locally advanced breast cancer patients receiving chemotherapy," Clin. Cancer Res. **19**(8), 2163–2174 (2013).
[38]A. Sadeghi-Naini, O. Falou, and G. J. Czarnota, "Quantitative ultrasound spectral parametric maps: Early surrogates of cancer treatment response," in *Proceedings of the 34th Annual International Conference of the IEEE Engineering in Medicine and Biology Society (EMBC), San Diego, CA, 2012* (IEEE, Washington, DC, 2012), pp. 2672–2675.
[39]A. Sadeghi-Naini, O. Falou, and G. J. Czarnota, "Quantitative ultrasound visualization of cell death: Emerging clinical applications for detection of cancer treatment response," in *Proceedings of the 34th Annual International Conference of the IEEE Engineering in Medicine and Biology Society (EMBC), San Diego, CA, 2012* (IEEE, Washington, DC, 2012), pp. 1125–1128.